Journal of Energy Resources Technology, Part B: Subsurface Energy and Carbon Capture
asmedigitalcollection.asme.org | Journal archive available at: https://asmedigitalcollection.asme.org/energyresources

A New Five-step Method for Advanced Evaluation of Shale Gas Formations and a Field Case Study of Marcellus Shale

Levent Taylan
Ozgur Yildirim[1]
Department of Energy and Mineral Engineering,
The Pennsylvania State University,
University Park, PA 16802
e-mail: lty104@psu.edu

John Wang
Department of Energy and Mineral Engineering,
The Pennsylvania State University,
University Park, PA 16802
e-mail: jb8474@psu.edu

Derek Elsworth
Department of Energy and Mineral Engineering,
The Pennsylvania State University,
University Park, PA 16802
e-mail: elsworth@psu.edu

This paper presents a new five-step method to evaluate shale gas formations with intricate pore networks. The method overcomes challenges posed by traditional workflows through an improved workflow and a new unconventional petrophysical model: (a) the new model accurately defines components of shale gas formations, including effective and isolated pores occupied by free and adsorbed gas; (b) total organic carbon (TOC) is evaluated using three techniques using conventional well logs to determine which techniques are more accurate; and (c) the improved method provides integrated evaluation of geomechanical properties, resources in place, and selection of stimulation candidate. Our field case study on Marcellus shale shows that (a) density-based TOC technique is more accurate and average TOC in the study area is 2.8%; (b) density porosity model is more reliable and average porosity in the study area is 8.5%. Positive correlation between TOCs and porosities in the upper and lower Marcellus suggests that effective pores contribute more significantly to the pore network than isolated pores; (c) gas in place is 120 Bcf with 60% free gas for a drilling unit of 640 acres. Large contrasts in Young's modulus (1 million psi) and minimum in situ stress (893 psi) along the upper Marcellus-Stafford limestone boundary, and resistivity separations in the lower Marcellus member, show that the upper Marcellus is a good stimulation candidate. This method and field case study provide valuable insights to evaluate Marcellus shale reservoirs and improve economic recovery of the resources in place. [DOI: 10.1115/1.4066417]

Keywords: oil/gas reservoirs, petroleum engineering, unconventional petroleum

1 Introduction

Shales are fine-grained, laminated, fissile sedimentary rocks composed primarily of clay, quartz, and feldspar. Shale gas formations contain gas-prone kerogen, derived from woody terrestrial plants. Traditionally, shale formations have been considered as seal and/or source rocks of a petroleum system. However, organic-rich shales are recently considered as unconventional reservoir rocks and provide additional source of energy. The advent of horizontal drilling and hydraulic fracturing treatments has made the economical production of Marcellus shale gas formations viable [1–3].

The Marcellus shale was deposited over 2 million years in anoxic deep marine depositional settings during the Middle Devonian. The orogenic events caused tectonic subsidence in the basin which created accommodation space for the Marcellus shale to be deposited during the Middle Devonian [4]. From bottom to top, the lower Marcellus, Cherry Valley, and upper Marcellus members are encompassed by the Marcellus shale which is the oldest unit of the Hamilton Group [5]. The Marcellus shale consists of black, organic-rich, fissile, pyrite-bearing shale intercalated with calcareous shale or dark-gray argillaceous limestone [6]. The Marcellus shale has 6 wt% average total organic carbon (TOC) and 6% average porosity [7]. The Marcellus shale overlies the Onondaga limestone and underlies the Stafford limestone member of the Skateaneles Formation [5,6].

Conventional petrophysical models are developed to evaluate conventional formations, such as sandstones and carbonates, in which non-clay minerals dominate and interconnected (or effective) pores are occupied by hydrocarbons and/or water. Gamma ray logging is typically used to help identify lithology and estimate volume percentage of shale. Density-neutron and sonic-neutron cross plots are used to evaluate porosity. Water saturation is evaluated using a Pickett plot or directly through the Archie equation [8]. Although these methods are successfully applied to conventional formations, evaluation of unconventional formations (i.e., shale gas) requires improved models and workflows.

Table 1 shows the outcomes of previous petrophysical workflows, models, and case studies for shale formations over the last decade. Lithofacies modeling of the Marcellus shale has been performed based on petrophysical, geomechanical, and geochemical data using core analysis and well logging [9]. The organic matter pore network occupying the free gas and adsorbed gas within

[1]Corresponding author.

Contributed by the Petroleum Division of ASME for publication in the Journal of Energy Resources Technology Part B: Subsurface Energy and Carbon Capture. Manuscript received June 1, 2024; final manuscript received August 17, 2024; published online January 10, 2025. Assoc. Editor: Tatiana Morozyuk.

Table 1 Previous petrophysical workflows, models, and case studies for shale gas formations

Formation	Materials	Methods	Findings	References
North American shale gas plays	Shale cuttings	FIB/SEM imaging to evaluate free and adsorbed gas in organic matter	Adsorbed CH_4 follows monolayer Langmuir model	[10]
Organic-rich shales	Core and log data	Petrophysical workflow and model	High surface area of clays complicates porosity evaluation in shales	[16]
North American shale plays	Core and log data	Petrophysical model to evaluate kerogen porosity	The model works well when TOC > 2%	[11]
Shale gas formations	Core and log data	Petrophysical model and workflow	Logs and isotherm tests are essential to calculate gas in place	[7]
Marcellus shale	Core, log, and seismic data	3D lithofacies modeling	Lithofacies are strongly influenced by organic matter, clays, and ratio of quartz and carbonate	[9]
Muskawa, Otterpark, and Evie shales	Core and log data	Volume of clay, porosity, water saturation evaluation	Elastic properties could be used to calculate porosity, clay volume, and water saturation	[18]
Marcellus shale	Geological, reservoir, and fluid data	Numerical modeling to investigate hydraulic fracturing propagation	A finite volume method could capture 3D geomechanical changes in hydraulic fractures	[12]
Marcellus shale	Core, log, and microseismic data	Petrophysical and geomechanical evaluation	Understanding the effect of horizontal stresses on fracture propagation is essential	[13]
Longmaxi, Niutitang shales	Core samples	Evaluate pore structure—helium pycnometry and pulse decay permeability	Pore structure is influenced by initial imbibition rate and normalized imbibed volume of fracturing fluid	[14]
Longmaxi shale	Log and cutting data	Organic matter and clay porosity evaluation using well logs and SEM images	Organic matter contributes more to shale pore volume than minerals	[15]

shale gas formations has been studied using focused ion beam (FIB)/scanning electron microscope (SEM) imaging technology [10]. A petrophysical model for shales that defines organic and inorganic pores has been proposed to solve for kerogen porosity [11]. Hydraulic fracturing in shale gas formations has been studied using various methods, including, but not limited to, numerical modeling [12], petrophysical analysis [13], and experimental techniques [14]. Nevertheless, petrophysical workflows and models to evaluate the shale formations based on wireline logs and core analysis are limited to a few studies [7,15–18].

Petrophysical evaluation of shale gas formations remain a challenge due to the organic matter, clay minerals, and complex pore networks at the nano-scale present in shale gas formations. To date, there is a lack of an integrated petrophysical evaluation of shale gas formations. This paper provides a new method and an improved model that accurately evaluate all components of shale gas formations, including non-clay minerals, clay minerals, organic matter, and effective and isolated pore space occupied by free and adsorbed gas. We then applied this method through a field case study Marcellus shale and provide insights on how to apply to the new method.

2 Materials

Figure 1 shows a well log data acquired from a well that penetrated the lower Marcellus member, upper Marcellus member, and Stafford limestone, from bottom to top, in a Marcellus shale field. The Cherry Valley member is absent in this study. The Marcellus shale interval is within the dry gas window with ~97% methane (CH_4). The well log data in Fig. 1 and input parameters in Table 2 are to evaluate the petrophysical properties of the Marcellus shale.

Porosity logs used in this study are bulk density and sonic logs. Since the well was drilled with air as the drilling fluid, the intervals penetrated during drilling were free from filtrate. Compressional and shear slowness logs were used as proxies for sonic log data in the Marcellus shale interval as sonic logs cannot be acquired in an air drilled well. The induction logging device measures formation resistivity as air is non-conducive.

In this study, X-ray diffraction (XRD) bulk mineralogy of 14 Marcellus shale samples from two wells [19] were used for the Marcellus shale gas formation. The average bulk mineralogy (wt%) of the 14 Marcellus shale samples is illite (40.7%), quartz (32.2%), K-feldspar (6.9%), pyrite (6.2%), calcite (4.7%), plagioclase (3.8%), dolomite (2.7%), chlorite (2.3%), kaolinite (0.2%), and others (0.3%) [19]. The presence of pyrite increases the density of the Marcellus shale. The average compressional travel time and density of clay and non-clay minerals of the Marcellus shale in this study were calculated using the compressional wave travel time [20,21] and density [22,23] of each mineral present in the Marcellus shale and relative abundances of minerals in the Marcellus shale [19] (Table 2). Additionally, an average value of the compressional travel time of organic matter, 167.5 μs/ft, was used for the Marcellus shale [24]. Density of organic matter in the Marcellus shale was calculated using vitrinite reflectance [25].

Biot poroelastic coefficient was calculated using the average depth for the Marcellus shale in the studied well and the overburden stress gradient in the study area. [26] constructed a correlation of overburden stress and Biot poroelastic coefficient for different shale formations using uniaxial strain measurements. Applying the linear regression equation of Ref. [26], we calculated the Biot poroelastic coefficient as 0.40 for the Marcellus shale. Additionally, the minimum in situ stress of the Stafford limestone was calculated using an average Biot poroelastic coefficient for Mississippian Indiana limestone which is 0.69 as discussed by Hart and Wang [27]. Bulk density values (~2.70 g/cm^3) indicate high levels of calcium carbonate in the Stafford limestone [5] similar to Indiana limestone which consists of 98% calcium carbonate [27] (Table 2).

Overburden stress and reservoir pressure were calculated based on overburden stress and reservoir pressure gradients of the Marcellus shale. A 1.17 psi/ft value of average overburden stress gradient from 15 Marcellus shale wells [28] was used in this study. Moreover, an average reservoir pressure gradient of 0.68 psi/ft of organic lean and organic-rich intervals of the Marcellus shale from three wells [29] was used. Density and compressional travel time through CH_4 were calculated based on reservoir pressure and temperature [30]. The gas deviation and formation volume factors were calculated using temperature and pressure at reservoir conditions and standard conditions for the zone of interest. Adsorbed gas storage in the Marcellus shale was calculated using Langmuir pressure (500 psi) and volume (200 Scf/ton) values that were reported by Yu and Sepehrnoori [31] (Table 2).

Based on geological studies and the laboratory evaluation of the Marcellus shale in the study area, volume of clay and water saturation (S_w) are 0.4 and zero for the Marcellus shale, respectively. The studied interval does not consist of free water (Table 2).

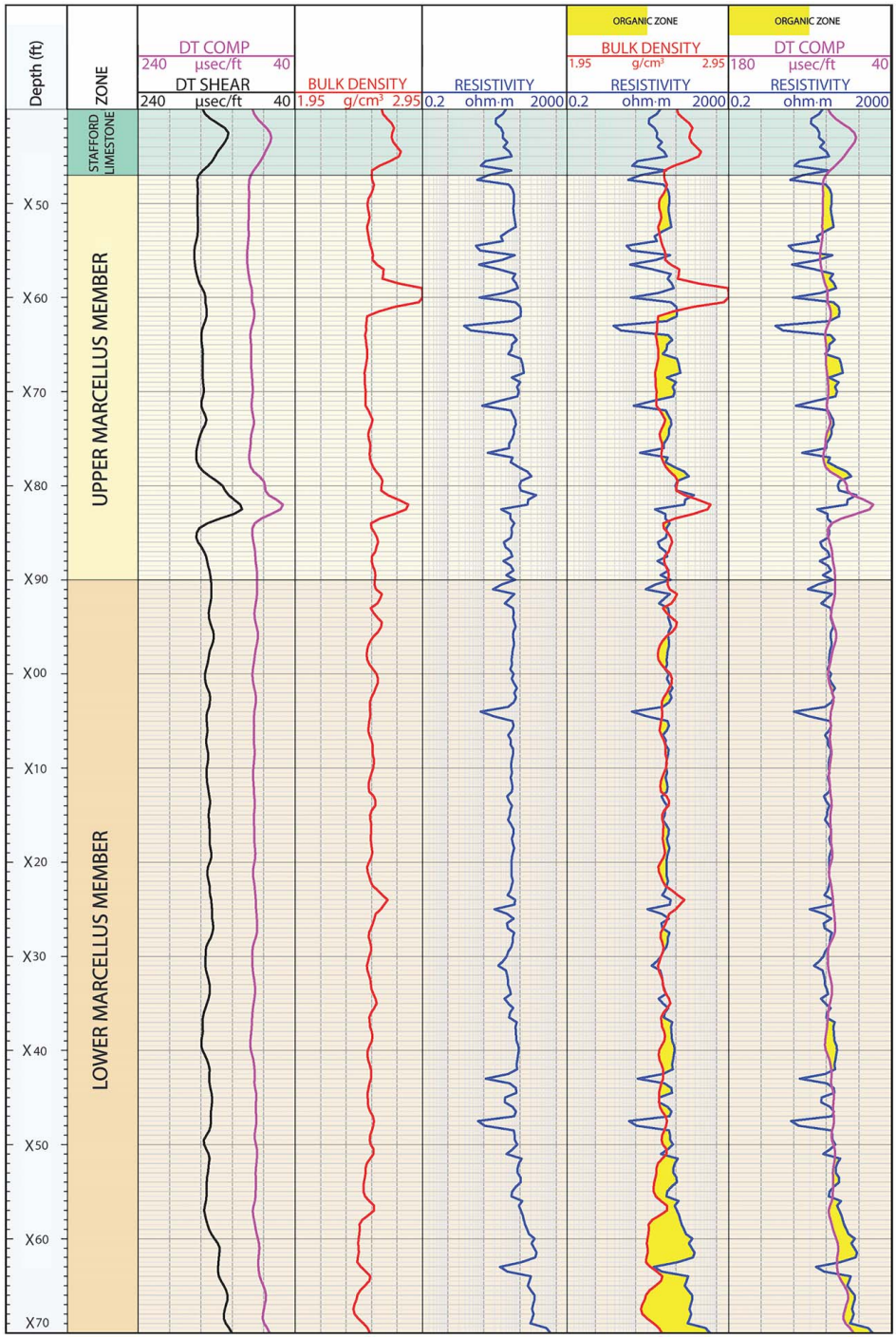

Fig. 1 Raw log for the Marcellus shale well, including the lower Marcellus member, upper Marcellus member, and Stafford limestone from bottom to top

3 Methods

Through our research and practical experiences in evaluating different geological formations, we developed a new method, including an improved workflow (Fig. 2) and a new unconventional petrophysical model (Fig. 3), to evaluate unconventional shale gas formations. Figure 2 shows an improved and integrated workflow to evaluate petrophysical properties of shale gas formations using conventional well logs. Figure 3 shows an improved unconventional petrophysical model that describes all partitions of shale gas formations.

The new method could be applied in five steps: (a) to understand the petrophysical model as discussed in step 1; (b) to evaluate maturity and TOC as discussed in step 2; (c) to evaluate porosity as discussed in step 3; (d) to evaluate geomechanical properties as discussed in step 4; and (e) to evaluate resources in place and application to stimulation as discussed in step 5.

3.1 Petrophysical Model (Step 1). Conventional petrophysical models have been used to evaluate the petrophysical properties of highly porous and permeable reservoirs, such as sandstones and limestones, that mainly contain non-clay minerals, water, and free hydrocarbons. Shale gas formations, formerly known as source rocks, have a complex pore network with the presence of organic matter, clay minerals, and adsorbed gas. In fact, improved

Table 2 Input parameters to evaluate the Marcellus shale gas formation

Parameters	Values	References
Cross-sectional area of the reservoir	2.79×10^7 ft^2 (640 acres)	This study
Thickness of the reservoir	123 ft	
Gas composition	~97% CH_4	
Reservoir pressure range	3637–3720 psi	
Reservoir temperature	572 °R (112 °F)	
Average gas deviation factor	0.896	
Average formation volume factor	4.6×10^{-3} ft^3/Scf	
Volume of clay (V_{Cl})	0.4	
Water saturation	0	
Average reservoir pressure gradient	0.68 psi/ft	[29]
Average overburden stress gradient	1.17 psi/ft	[28]
Density of clay minerals	2.81 g/cm^3	[23]
Density of non-clay minerals	2.91 g/cm^3	[22,23]
Density of organic matter	1.32 g/cm^3	[25]
Compressional travel time of clay minerals	52.30 μs/ft	[20]
Compressional travel time of non-clay minerals	47.12 μs/ft	[21]
Compressional travel time of organic matter	167.5 μs/ft	[24]
Density of CH_4	0.171 g/cm^3	[30]
Compressional travel time of CH_4	606.36 μs/ft	
Biot poroelastic coefficient (Marcellus shale)	0.4	[26]
Biot poroelastic coefficient (Stafford limestone)	0.69	[27]
Level of organic metamorphism (Marcellus shale)	10.5	[33]
Level of organic metamorphism (Stafford limestone)	5	[33]
Langmuir pressure	500 psi	[31]
Langmuir volume	200 Scf/ton	

petrophysical models have been necessary to evaluate the petrophysical properties of these formations [16]. Therefore, we propose an improved unconventional petrophysical model (modified from Ref. [16]) for shale gas formations to overcome challenges of inaccurate evaluation with existing petrophysical models which do not specifically evaluate organic matter, adsorbed gas, and clay minerals. Our petrophysical model accurately defines solid matrix and effective and total pore space of shale gas formations that are occupied by water, free gas, and adsorbed gas (Fig. 3).

From a petrophysical standpoint, shale gas formations are composed of solid matrix and pore space filled by fluids. Solid materials comprising the matrix include non-clay minerals, clay minerals, and organic matter. The porosity of organic matter is oil wet. The remainder of the pore space is water wet. Adsorbed gas and clay-bound water occupy the ineffective pores. Adsorbed gas is trapped on the pore walls of the organic matter. Effective porosity is composed of dead-end pores and interconnected pores, forming a network. Interconnected pores are occupied by mobile water and free gas. Dead-end pores are occupied by free gas in organic pores and capillary-bound water. The mobile water (or free water) remains mobile in the interconnected pore space. The water phase remains immobile at the water saturation of clay- and capillary-bound waters [7,11].

The volume of clay minerals comprises extremely fine-grained solid clay with its porosity occupied by clay-bound water. Conversely, the volume of non-clay minerals is the volumetric sum of minerals such as quartz, calcite, and plagioclase with the pore space occupied by mobile water and free gas. Similarly, the total of the solid organic matter and its pore space is occupied by adsorbed and free gas. Shale gas formations consist of inorganic and organic partitions. The organic partition consists of organic matter, adsorbed and free gas whereas the inorganic partition consists of clay and non-clay minerals and water [11,16].

The non-clay minerals of the matrix are mainly quartz, feldspar, carbonates, and iron oxides. The primary clay minerals are illite,

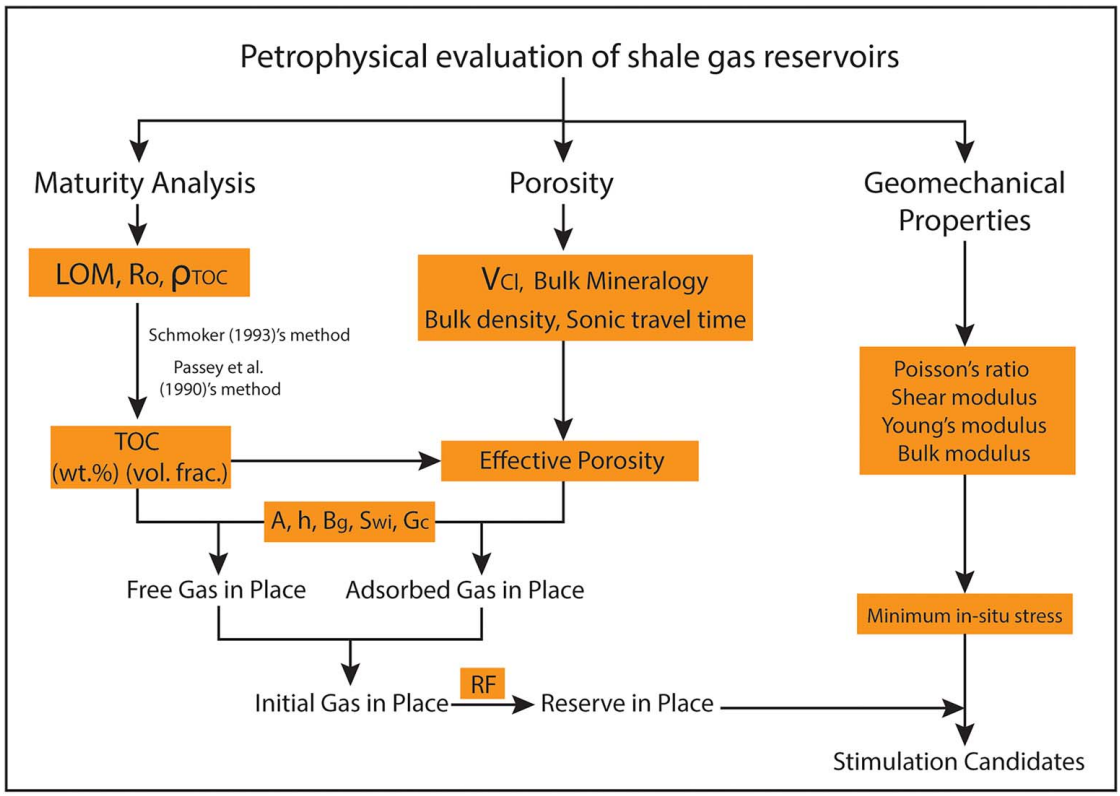

Fig. 2 Methodology of petrophysical evaluation of shale gas formations

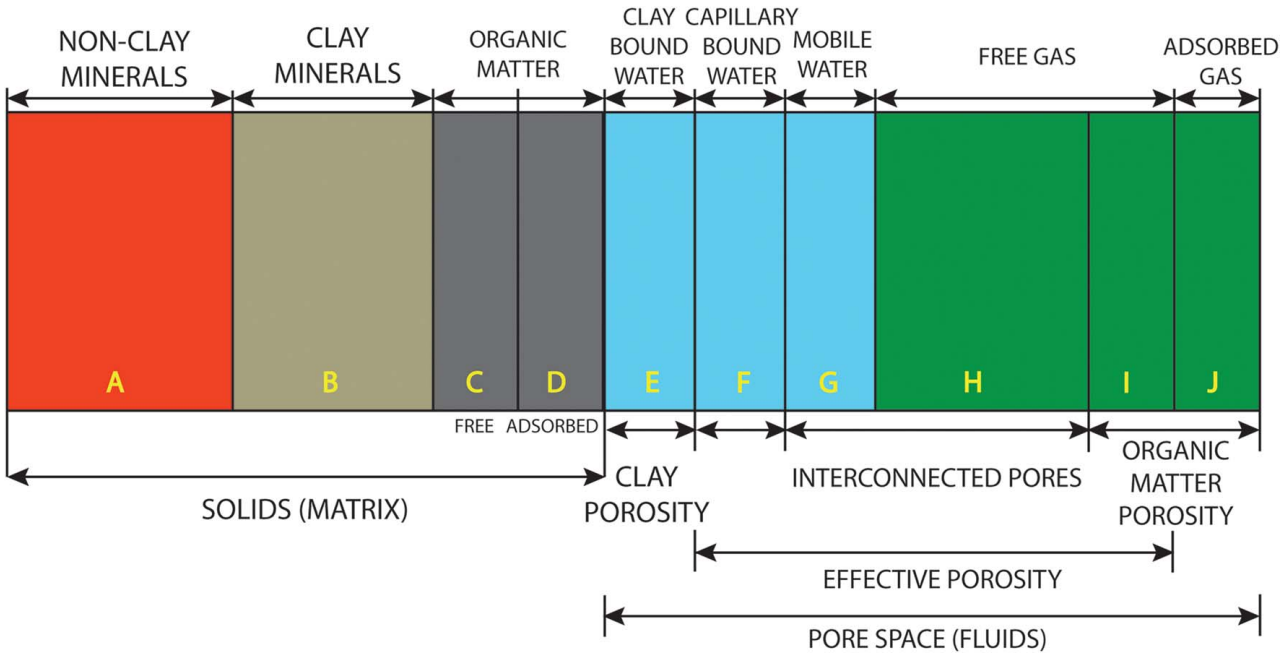

Fig. 3 Schematic petrophysical model of shale gas formations (modified from Ref. [16])

kaolinite, smectite, chlorite, and glauconite. Organic matter of shales comprises kerogen, bitumen, pyrobitumen, and char [16]. Porosity within clay minerals is ineffective and is typically occupied by clay-bound water. Inorganic non-clay minerals also contain capillary-bound and mobile water. The adsorbed gas is trapped on the pore walls of solid organic matter. Free gas accumulates within the pore space of the organic matter and inorganic partitions of the matrix such as non-clay minerals [7].

3.2 Maturity Analysis (Step 2). The maturity analysis includes analyses of vitrinite reflectance, density of organic matter, and TOC (Fig. 2). In the absence of direct laboratory analysis of TOC, correlations could be applied. Vitrinite reflectance of shale gas formations could be calculated using an empirical equation developed from the laboratory evaluation of the level of organic metamorphism (LOM) [32]. Density of organic matter could be calculated based on vitrinite reflectance of core samples analyzed in the laboratory [25]. Three different TOCs (wt% and vol. frac.) could be calculated with sonic/resistivity and density resistivity overlay methods [33] and density-based modified Schmoker's [34] method. For the Marcellus shale case study, our TOC calculation methodology was verified using the methodology to calculate the TOC of the Stafford limestone. Once applied and validated through case studies, one could develop understanding of how to fine tune the three TOC evaluation techniques and which one is more accurate and applicable in practice.

3.2.1 Vitrinite Reflectance and Density of Organic Matter. In this study, vitrinite reflectance, R_o, was calculated using an LOM of 10.5 since TOC of overmature shale gas formations is underestimated if the resistivity/density and resistivity/sonic overlay methods are applied with LOM values above 10.5 [16]. For immature carbonates such as the Stafford limestone, an LOM of 5 was used to evaluate the organic maturity [33]. Vitrinite reflectance, R_o, was calculated using Eq. (1) developed by Lecompte et al. [32] as

$$R_o = -0.0039\text{LOM}^3 + 0.1494\text{LOM}^2 - 1.5688\text{LOM} + 5.5173 \quad (1)$$

where R_o is the vitrinite reflectance and LOM is the level of organic metamorphism.

Density of organic matter for Marcellus shale was calculated based on R_o as in Eq. (2) [25].

$$\rho_{\text{TOC}} = 0.972 + 0.342R_o \quad (2)$$

where ρ_{TOC} is the density of organic matter (kerogen) and R_o is the vitrinite reflectance.

3.2.2 Total Organic Carbon. The TOC could be calculated using Passey et al. [33] and modified Schmoker's [34] methods. The TOC and density of organic matter were then used in the porosity and gas in place calculations since the TOC correlates directly with quantification of porosity and bulk volume of gas [16].

The resistivity separation ($\Delta \log R$) method of Passey et al. [33], overlay of porosity and resistivity logs, was utilized to calculate the TOC as wt%. Organic-rich intervals exhibit resistivity separation due to the presence of low-velocity and low-density kerogen. Inorganic intervals do not exhibit resistivity separation; therefore, the resistivity, sonic and density baseline values were assigned in inorganic intervals where no resistivity separation exists between the resistivity and porosity curves. The expressions for calculating $\Delta \log R$ using porosity (sonic and density)/resistivity overlay methods can be written as follows in Eqs. (3)–(5) [33] with the expressions to calculate TOC (wt%) using $\Delta \log R$:

$$\Delta \log R_S = \log_{10}(R/R_B) + 0.02(\Delta t - \Delta t_B) \quad (3)$$

$$\Delta \log R_D = \log_{10}(R/R_B) - 2.5\,(\rho_b - \rho_B) \quad (4)$$

$$\text{TOC}_{S,D} = \Delta \log R_{S,D} \times 10^{2.297 - 0.1688\text{LOM}} \quad (5)$$

where $\Delta \log R_S$ and $\Delta \log R_D$ ($\Delta \log R_{S,D}$) are curve separations between resistivity and sonic and density porosity logs measured in logarithmic resistivity cycles. R is the true formation resistivity. R_B is the resistivity on Δt_B when curves are baselined in clay rich rocks. Δt is the sonic log reading. Δt_B is the compressional transit time over the inorganic baseline interval. ρ_b is the bulk density. ρ_B is the bulk density value of the baseline. $\text{TOC}_{S,D}$ is the total organic carbon recovered from resistivity and sonic and density porosity log overlays. LOM is the level of organic metamorphism.

For the zone of interest in the Marcellus shale, the resistivity and porosity curves were baselined in the upper part of the lower

Marcellus member where there is no resistivity separation in the sonic/resistivity overlay method. These baseline values are 57.42 ohm m for the resistivity, 93.14 μs/ft for the compressional travel time, and 2.56 g/cm^3 for the bulk density. The percentage of negative values in density–resistivity separation ($\Delta \log R$) and TOC values of the zone of interest are 45%, 39%, and 6% for the sonic/resistivity and density/resistivity overlay methods, and the density-based method, respectively. The negative values indicate zero TOC in these intervals. Therefore, the negative values were corrected to be zero. The calculations of the other petrophysical properties were performed based on the TOC data that are free of negative values.

Schmoker [34] derived an equation to calculate TOC of Devonian shale gas formations based on bulk density log and density of inorganic gray shales from 74 intervals in 12 wells. The TOC values calculated from this equation were compared with laboratory measurements of TOC of core samples. Schmoker [34] assumes 1.0 g/cm^3 value for the density of the organic matter. The constant, 55.822, in Schmoker's [34] TOC (wt%) equation is directly proportional to the organic matter density. For the Marcellus shale case study, the density of organic matter is 1.32 g/cm^3. Therefore, we modified the constant based on the density of organic matter for the Marcellus shale. The average calculated density value of inorganic intervals that do not show resistivity separations in the Marcellus shale is 2.64 g/cm^3. Additionally, the Stafford limestone exhibits higher bulk density values compared to the Marcellus shale and does not exhibit any resistivity separation. Therefore, the density of the inorganic intervals in the Stafford limestone is equal to bulk density values. We calculated the TOC of the Marcellus shale and Stafford limestone from the bulk density logs using Eq. (6) (modified from Ref. [34]).

$$\mathrm{TOC} = 73.406\left[\left(\frac{\rho_{\mathrm{in}}}{\rho_b}\right) - 1\right] \tag{6}$$

where TOC is the total organic carbon, ρ_b is the bulk density log reading, and ρ_{in} is the density of inorganic intervals.

The expression for calculating V_{TOC} that was used in the porosity calculations can be written as follows:

$$V_{\mathrm{TOC}} = \rho_b \mathrm{TOC}/\rho_{\mathrm{TOC}} \tag{7}$$

where V_{TOC} is the volume of organic matter, ρ_{TOC} is the density of organic matter, and TOC is the total organic carbon.

3.3 Porosity Evaluation (Step 3). Effective porosity of shale gas formations could be interpreted using sonic and density logs. These tools give bulk density and compressional travel time of the penetrated geological formation. Therefore, for the Marcellus shale, the porosity was estimated indirectly using measured bulk density and compressional travel time data and those of minerals present in the Marcellus shale—namely, bulk mineralogy, volume of clay, and TOC (wt% and vol. frac.) from the density/resistivity and sonic/resistivity overlay methods, and the density-based method (Fig. 2). The effective porosity was estimated based on the petrophysical model that takes the clay minerals, non-clay minerals, organic matter, and fluid partitions of the shale gas formations into account using compressional travel times, bulk density, and TOC (vol%) values of the partitions (Fig. 3).

The pore space is subdivided into three components: namely, clay porosity, effective porosity, and porosity of organic matter based on the assumption that organic pores are isolated and dead-end in shale as expressed below with respect to the petrophysical model in Fig. 3 [11,16]. The expressions to calculate the clay porosity, effective porosity, porosity of organic matter, and total porosity can be written as follows in Eqs. (8)–(11) based on the shale gas petrophysical model (modified from Ref. [16]):

$$\phi_{\mathrm{Tot}} = \phi_{\mathrm{Cl}} V_{\mathrm{Cl}} + \phi_{\mathrm{Eff}} + \phi_{\mathrm{TOC}_A} V_{\mathrm{TOC}_A} \tag{8}$$

$$\phi_{\mathrm{Cl}} = \frac{V_{P,\mathrm{Cl}}}{V_{\mathrm{Cl}}} = \frac{V_E}{V_B + V_E} \tag{9}$$

$$\phi_{\mathrm{TOC}_A} = \frac{V_{P,\mathrm{TOC}_A}}{V_{\mathrm{TOC}_A}} = \frac{V_J}{V_D + V_J} \tag{10}$$

$$\begin{aligned}\phi_{\mathrm{Eff}} &= \phi_{\mathrm{Tot}} - \phi_{\mathrm{Cl}} V_{\mathrm{Cl}} - \phi_{\mathrm{TOC}_A} V_{\mathrm{TOC}_A} \\ &= \frac{V_F + V_G + V_H + V_I}{V_A + V_C + V_F + V_G + V_H + V_I}\end{aligned} \tag{11}$$

where ϕ_{Tot} is the total porosity. ϕ_{Cl} is the clay porosity. ϕ_{TOC_A} is the organic matter porosity that is occupied by adsorbed gas. ϕ_{Eff} is the effective porosity. V_{Cl} is the volume of clay minerals. V_{TOC_A} is the volume of organic matter whose pore space is occupied by adsorbed gas. $V_{P,\mathrm{Cl}}$ is the volume of pore space in clay minerals. V_{P,TOC_A} is the volume of pore space in the organic matter whose pore space is occupied by adsorbed gas. $V_A, V_B, \ldots, V_J$ are the volumes of fractions of solids and pore space in a shale gas reservoir.

Density logging evaluates the porosity of the formation depending on the bulk density of the zone of interest. Bulk density and density porosity can be calculated from Eqs. (12) and (13) (modified from Ref. [35]). Density porosity was calculated using TOC (vol. frac.) that is calculated based on the resistivity/density and resistivity/sonic overlay methods, and the density-based method. Compressional and shear waves travel within the shale formation during sonic logging. They traverse different fractions of the rock so that travel time and sonic porosity of different partitions can be calculated by Eqs. (14) and (15) (modified from Ref. [36]). Sonic porosity was calculated using TOC (vol. frac.) that is calculated based on separation between sonic and resistivity logs.

$$\rho_b = \phi_{\mathrm{Den}}\rho_F + V_{\mathrm{TOC}}\rho_{\mathrm{TOC}} + V_{\mathrm{Cl}}\rho_{\mathrm{Cl}} + (1 - V_{\mathrm{Cl}} - V_{\mathrm{TOC}} - \phi_{\mathrm{Den}})\rho_{\mathrm{Ncl}} \tag{12}$$

$$\phi_{\mathrm{Den}} = \frac{\rho_{\mathrm{Ncl}} + V_{\mathrm{TOC}}(\rho_{\mathrm{TOC}} - \rho_{\mathrm{Ncl}}) + V_{\mathrm{Cl}}(\rho_{\mathrm{Cl}} - \rho_{\mathrm{Ncl}}) - \rho_b}{\rho_{\mathrm{Ncl}} - \rho_F} \tag{13}$$

$$\begin{aligned}\Delta t = {} & \Delta t_F \phi_{\mathrm{Son}} + \Delta t_{\mathrm{Cl}} V_{\mathrm{Cl}} + \Delta t_{\mathrm{TOC}} V_{\mathrm{TOC}} \\ & + (1 - V_{\mathrm{Cl}} - V_{\mathrm{TOC}} - \phi_{\mathrm{Son}})\Delta t_{\mathrm{Ncl}}\end{aligned} \tag{14}$$

$$\phi_{\mathrm{Son}} = \frac{\Delta t_{\mathrm{Ncl}} + V_{\mathrm{Cl}}(\Delta t_{\mathrm{Cl}} - \Delta t_{\mathrm{Ncl}}) + V_{\mathrm{TOC}}(\Delta t_{\mathrm{TOC}} - \Delta t_{\mathrm{Ncl}}) - \Delta t}{\Delta t_{\mathrm{Ncl}} - \Delta t_F} \tag{15}$$

where V_{Cl} is the volume of clay minerals. V_{TOC} is the volume of organic matter. ρ_b is the bulk density. ϕ_{Den} is the density porosity. ρ_F is the fluid density. ρ_{TOC} is the density of the organic matter. ρ_{Cl} is the density of the clay minerals. ρ_{Ncl} is the density of the non-clay minerals. Δt is the sonic log reading. Δt_F is the sonic log reading in fluids. ϕ_{Son} is the sonic porosity. Δt_{Cl} is the sonic log reading in clay minerals. Δt_{TOC} is the sonic log reading in organic matter. Δt_{Ncl} is the sonic log reading in non-clay minerals.

3.4 Geomechanical Properties (Step 4). Geomechanical properties of shale gas formations, such as Poisson's ratio, shear modulus, Young's modulus, and bulk modulus, are calculated based on compressional and shear travel times of sound waves in different partitions of shale gas formations from sonic logging (Fig. 2) as in Eqs. (16)–(19). The geomechanical properties along with minimum in situ stress can be used to help select stimulation candidates. Minimum in situ stress is primarily affected by Poisson's ratio, Biot poroelastic coefficient, overburden stress, and reservoir pressure as shown in Eq. (20). Tectonic stress can affect the minimum in situ stress in tectonically active regions [37]. Hydraulic

fracturing strategies are further optimized based on geomechanical properties. The minimum in situ stress and Young's modulus are important factors regulating fracture vertical height growth depending on the relationship between the values at lower and upper boundaries and inside the zone of interest [38,39].

$$v = \frac{0.5(\Delta t_s/\Delta t_c)^2 - 1}{(\Delta t_s/\Delta t_c)^2 - 1} \tag{16}$$

$$G = 1.34 \times 10^{10} \frac{\rho_b}{\Delta t_s^2} \tag{17}$$

$$E = 2G(1 + v) \tag{18}$$

$$K = 1.34 \times 10^{10} \rho_b \left(\frac{1}{\Delta t_c^2} - \frac{4}{3\Delta t_s^2} \right) \tag{19}$$

$$\sigma_{\min} = \frac{v}{1 - v}(\sigma_{ob} - p) + p + \sigma_{\text{tect}} \tag{20}$$

where v is the Poisson's ratio. Δt_s and Δt_c are the shear and compressional slowness. E is the Young's modulus. G is the shear modulus. K is the bulk modulus. ρ_b is the bulk density. σ_{ob} is the overburden stress. $\sigma_{\min}$ is the minimum in situ stress. p is the reservoir pressure. α is Biot poroelastic coefficient. σ_{tect} is the tectonic stress.

3.5 Initial Gas in Place and Technically Recoverable Resources (Step 5). Initial gas in place is composed of adsorbed gas, free gas, and dissolved gas. The gas dissolved into liquid hydrocarbons and formation water is negligible in the dry gas region. Adsorbed gas is determined through adsorption isotherm analyses. The adsorbed gas volume can be dominant over that of free gas if the shale formation has pores residing mostly inside the organic matter. In fact, the initial gas in place of the shale would be underestimated if the gas adsorbed on the organic pores is not considered. The gas in place of shale gas formations was calculated depending on adsorbed and free gas, trapped in the organic solid and inorganic pores, respectively, as in Eq. (21). Once the porosity, water saturation, thickness, cross-sectional area, and volume factor of the formation are known, free gas can be calculated using Eq. (23). The adsorbed gas storage in the shale was quantified by the Langmuir isotherm [40]—derived from crushed rock samples as in Eq. (24). Furthermore, adsorbed gas can be calculated using the cross-sectional area of the reservoir, thickness, bulk density, and adsorbed gas storage using Eq. (25). The technically recoverable portion of the initial gas in place was calculated based on a recovery factor as in Eq. (22) [7,10,41]. Stimulation candidates were determined based on the maturity analyses, porosity evaluation, and geomechanical properties of shale gas formations (Fig. 2).

Table 3 Average calculated TOC (wt%) and porosity values of the upper Marcellus member, lower Marcellus member, and Marcellus shale

Method	Sonic/resistivity overlay		Density/resistivity overlay		Density-based method	
Rock formation	TOC (wt%)	Porosity	TOC (wt%)	Porosity	TOC (wt%)	Porosity
Upper Marcellus	0.4	7.7	0.4	10.0	2.4	7.8
Lower Marcellus	0.3	7.2	0.7	11.5	3.0	8.8
Marcellus shale	0.3	7.4	0.6	11.0	2.8	8.5

$$G_t = G_f + G_a \tag{21}$$

$$G_r = G_t \text{RF} \tag{22}$$

$$G_f = 43,560 \times 10^{-9} Ah\phi_{\text{eff}} \frac{1 - S_w}{B_g} \tag{23}$$

$$G_c = \frac{V_l p}{p + P_l} \tag{24}$$

$$G_a = 1,359.65 \times 10^{-9}\ \text{Ah}\rho_b G_c \tag{25}$$

where G_t is the initial gas in place. G_f and G_a are the free and adsorbed gas in place. G_r is the technically recoverable resources. RF is the recovery factor. h is the thickness of the reservoir. A is the cross-sectional area of the reservoir. ϕ_{eff} is the effective porosity from the log and/or core data. B_g is the gas formation volume factor. S_w is the water saturation. G_c is the adsorbed gas storage. P_l is the Langmuir pressure. V_l is the Langmuir volume. p is the reservoir pressure. ρ_b is the bulk density. TOC is the total organic carbon. 43,560 is the conversion from ft^2 to acre. 1359.65 is the conversion from g/cm^3 to ton/acre-ft. 10^{-9} is the conversion factor from Scf to Bcf.

4 Field Case Study

A field case study of the Marcellus shale was conducted following our five-step methodology, beginning with the petrophysical model. The results of the subsequent steps are summarized in four sections: (a) maturity analysis, (b) porosity evaluation, (c) geomechanical properties, and (d) initial gas in place and technically recoverable resources. The average calculated TOC (wt%), porosity, geomechanical properties, as well as the gas in place values for the upper Marcellus member, lower Marcellus member, and Marcellus shale using the resistivity/density and resistivity/sonic overlay methods, and the density-based method are shown in Tables 3–5. The composite well log for this Marcellus shale well showing the Stafford limestone, the upper Marcellus member, and the lower Marcellus member includes the raw log, computed TOC, porosity, geomechanical properties, and technically recoverable resources logs (Fig. 4). In Fig. 4, shaded areas outlined with rectangles represent the stimulation candidates (Int_1, Int_2, and Int_3) for the Marcellus shale based on the TOC, porosity, geomechanical properties, and technically recoverable resources results.

4.1 Maturity Analysis. The vitrinite reflectance was calculated as 1% for an LOM of 10.5 for the Marcellus shale as suggested by Passey et al. [33]. The average TOC (wt%) for the Marcellus shale was calculated as 0.3% and 0.6% by sonic/resistivity and

Table 4 Average calculated geomechanical properties of the Stafford limestone, upper Marcellus member, lower Marcellus member, and Marcellus shale

	Poisson's ratio	Shear modulus (million psi)	Young's modulus (million psi)	Bulk modulus (million psi)	Minimum in situ stress (psi)
Stafford limestone	0.25	1.8	4.6	3.1	3747
Upper Marcellus	0.22	1.5	3.6	2.2	2854
Lower Marcellus	0.20	1.6	3.8	2.1	2730
Marcellus shale	0.21	1.5	3.7	2.2	2773

Table 5 Gas in place (Bcf) results using sonic/resistivity overlay, density/resistivity overlay, and the density-based methods for the Marcellus shale well

Gas in place/method		Sonic/resistivity overlay	Density/resistivity overlay	Density-based
Upper Marcellus	Free gas in place	23.44	30.38	23.60
	Adsorbed gas in place	17.32	17.32	17.32
	Initial gas in place	40.46	47.40	40.61
	Free gas %	58	64	58
	Reserve in place	4.05	4.74	4.06
Lower Marcellus	Free gas in place	41.11	65.14	50.12
	Adsorbed gas in place	31.30	31.30	31.30
	Initial gas in place	72.41	96.44	81.42
	Free gas %	57	68	62
	Reserve in place	7.24	9.64	8.14
Marcellus shale	Free gas in place	64.55	95.52	73.71
	Adsorbed gas in place	48.32	48.32	48.32
	Initial gas in place	112.87	143.84	122.03
	Free gas %	57	66	60
	Reserve in place	11.29	14.38	12.20

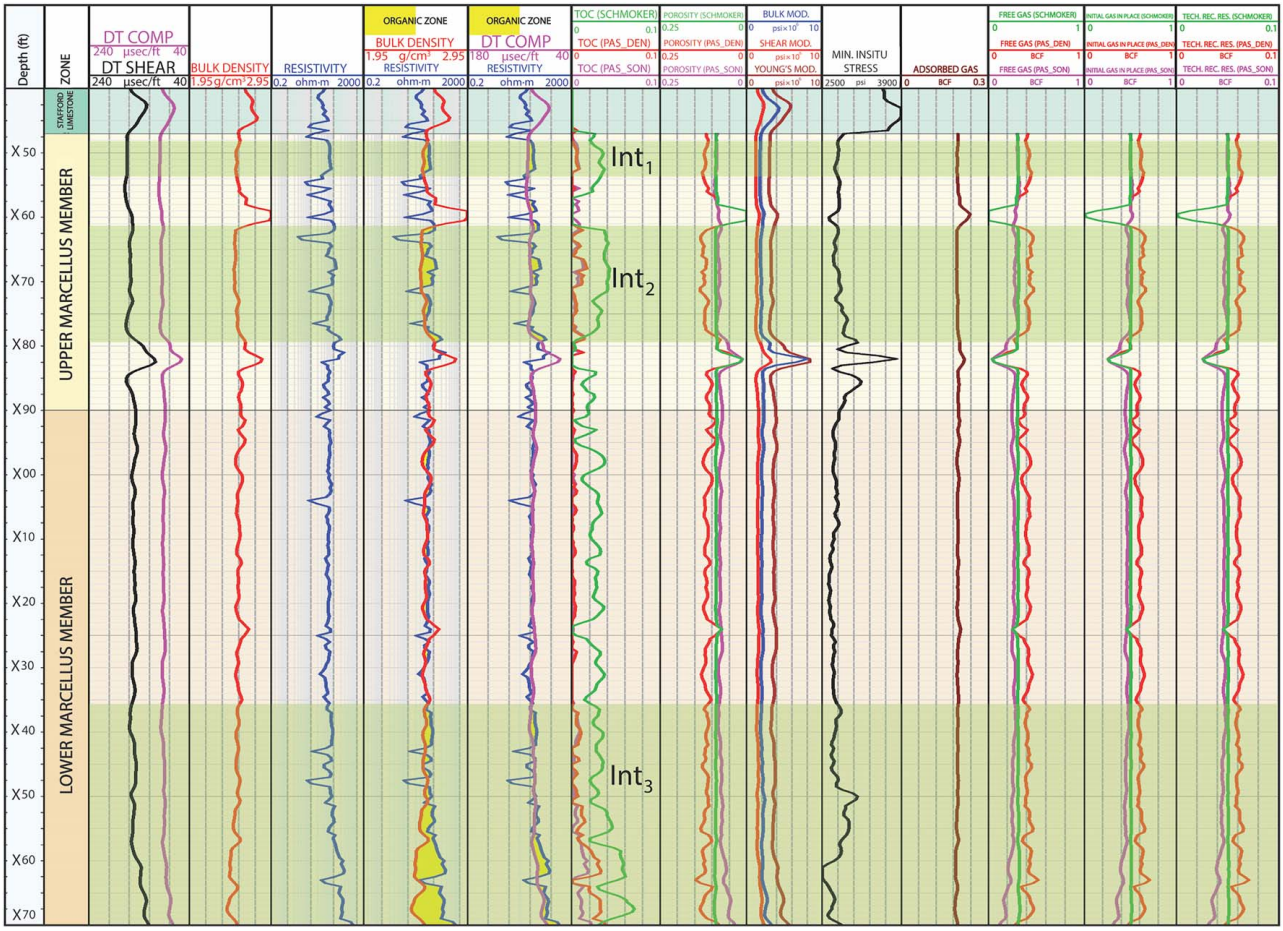

Fig. 4 Composite log of the Marcellus shale well. The shaded intervals represent stimulation candidates (Int_1, Int_2, and Int_3) for the Marcellus shale. PAS_DEN and PAS_SON represent density- and sonic/resistivity overlay methods. TECH. REC. RES. represents technically recoverable resources.

density/resistivity overlays in Eq. (5), respectively. The density-based method, on the other hand, shows a 2.8% average TOC for the Marcellus shale using Eq. (6). Additionally, the TOC of the Stafford limestone is 0%, 0.04%, and 0% for the sonic/resistivity and density/resistivity overlay methods, and the density-based method, respectively. This is confirmed with the scarcity of $\Delta \log R$ separations in the Stafford limestone (Fig. 1). Therefore, this shows that our TOC calculation methods are tested and verified.

The average TOC (vol%) that was calculated based on the organic matter density using Eq. (7) is 0.6 using the sonic/resistivity overlay method log, 1% using the density/resistivity overlay method, and 5.4% using the density-based method. The density of the organic matter used in these calculations was derived from the kerogen density and vitrinite reflectance relationship in Eq. (2) which was established based on the core analysis of the Marcellus shale [25]. Kerogen was taken as a reference to calculate ρ_{TOC} in

the Marcellus shale since both TOC and kerogen relate to the organic matter of the Marcellus shale. Using the calculated R_o of 1%, we estimated a ρ_{TOC} of 1.32 g/cm^3 for the zone of interest.

The resistivity/density and resistivity/sonic overlay methods show very low TOC (wt%) values that are lower than 1% although the Marcellus shale exhibits intervals with high resistivity separations. A 10.5 calibration limit of LOM and a correction multiplier were proposed to address potential underestimation of the TOC in overmature shale gas formations [16,17]. Although we took a value of 10.5 for LOM, very low TOC values were calculated using the resistivity/density and resistivity/sonic overlay methods. Despite its intricacy, the TOC was underestimated when the resistivity/density and resistivity/sonic overlay methods are applied in this study. However, the density-based method for TOC estimation demonstrated a simpler yet effective approach, resulting in an average TOC value of 2.8% for the Marcellus shale. This is consistent with high resistivity, low bulk density, and high acoustic travel time responses and hence high resistivity separations of organic-rich intervals in the studied Marcellus shale interval. A notable advantage of the density-based method lies in its derivation from well log data specifically obtained from Devonian shales, including the Marcellus shale. In fact, the density-based method is a more reliable approach for estimating TOC in the Marcellus shale compared to the resistivity/density and the resistivity/sonic overlay methods.

The average TOC (wt%) values are higher in the lower Marcellus member (3.0%) than the upper Marcellus member (2.4%) based on the density-based method (Table 3 and Fig. 4). The sonic/resistivity, density/resistivity, and density-based methods suggest that TOC (wt %) values approach 2.2%, 3.8%, and 7.1% at the bottom of the lower Marcellus member. The TOC results in the bottom of the lower Marcellus member conform to previous work suggesting TOC values that range from 2% to 10% [42] and that are 6% on average [7] in the Marcellus shale.

In summary, the density-based method is a more reliable approach to interpret TOC in the Marcellus shale compared to the resistivity/density and the resistivity/sonic overlay methods.

4.2 Porosity Evaluation. The two porosity models (Eqs. (13) and (15)) were applied and our evaluations are summarized in Table 3. A positive correlation exists between the TOC and porosity values of the upper and lower Marcellus members when the three TOC calculation techniques are applied (Table 3). Organic matter typically exhibits higher porosity than the shale matrix. Higher amounts of TOC in shales can lead to an increase in total porosity due to the low-density (and resulting low-velocity nature) of the organic matter. The majority of organic pores are effective. In fact, an increase in organic matter contributes to the effective porosity. Specifically, for the density-based method, the lower Marcellus shale exhibits an average TOC of ~3.0% and an average porosity of 8.8%, while the upper Marcellus shale shows an average TOC of 2.4% and an average porosity of 7.8%. This suggests that, in the Marcellus shale, the effective porosity contributes more significantly to the pore network than isolated pores.

The average sonic porosity of 7.4% is lower than the average density porosities of 8.5% and 11.0% from the density-based method and the resistivity/density overlay method, respectively. First, the difference between sonic and density derived porosities can be attributed to the fact that porosity is indirectly estimated from sonic travel time and bulk density measured through the formation using sonic and density logs. Second, sonic logging cannot fully detect all the porosity in the Marcellus shale due to the presence of extensive fractures which are discontinuities. Third, relatively low compressional slowness (avg. 91 μs/ft) was measured by sonic log for organic matter and gas bearing Marcellus shale. This measurement is close to the lower boundary of a range (60–200 μs/ft) proposed for compressional slowness of shales in Ref. [22]. In fact, relatively low compressional slowness yields relatively low sonic derived porosity as suggested by Eq. (15). Complex relations of porosity with travel time and geomechanical properties of the rock can play role on the difference unlike relatively simple relation between porosity, bulk density, and matrix density.

The density derived porosity (8.5%) in this study is higher than the 6% average porosity of Ref. [7] and 7% average porosity of Ref. [43]. Depending on actual or assumed bulk mineralogy of the Marcellus shale in the studied wells, different bulk density and matrix density values were used resulting in different porosity values in each study.

In summary, porosity of the Marcellus shale (8.5%) that was obtained using density-based model is more reliable than that from resistivity/density and resistivity/sonic overlay.

4.3 Geomechanical Properties. Geomechanical properties of the Marcellus shale were evaluated using the models presented in step 4 of our methodology. Tectonic stress is zero in the region. Average Poisson's ratio, shear modulus, Young's modulus, bulk modulus, and minimum in situ stress of the Marcellus shale are 0.21, 1.5 million psi, 3.7 million psi, 2.2 million psi, and 2773 psi, respectively. Table 4 summarizes our results for upper and lower Marcellus shale and Stafford limestone.

Our study shows that the Young's modulus and minimum in situ stress of the upper Marcellus member are 3.6 million psi and 2854 psi, respectively, while the Young's modulus and minimum in situ stress of the Stafford limestone are 4.6 million psi and 3747 psi, respectively. This indicates that there are distinct contrasts in minimum in situ stress and geomechanical properties, especially the Young's modulus along the upper Marcellus-Stafford limestone boundary and the lower portion of the upper Marcellus member (Fig. 4 and Table 4). This implies that the boundaries with higher in situ stresses will act as a barrier to prevent growth of fractures. Therefore, fracture propagation would be hindered along the upper Marcellus-Stafford limestone boundary and the lower portion of the upper Marcellus member with the larger minimum in situ stress and modulus contrasts [39].

The accuracy of measurements, such as compressional and shear slowness, and bulk density and assumptions such as overburden stress gradient and Biot poroelastic coefficient and pore pressure can introduce uncertainty in the calculations of geomechanical properties and minimum in situ stress. Mineral composition, porosity, and fluid properties of the Marcellus shale affect the compressional and shear slowness measurements.

In summary, geomechanical properties of the Marcellus shale can be evaluated using travel time of compressional and shear waves. The Marcellus shale was compared with overlying Stafford limestone in terms of geomechanical properties to select stimulation candidates.

4.4 Initial Gas in Place and Technically Recoverable Resources. Table 5 shows the gas in place calculated using the density/resistivity overlay, sonic/resistivity overlay, and the density-based methods for the upper Marcellus member, lower Marcellus member, and Marcellus shale, respectively. Average adsorbed gas storage via Langmuir isotherms for density and sonic log is 176.1 Scf/ton for the zone of interest using Eq. (24). Gas in place from the density-based method is more reliable since the resistivity/density and resistivity/sonic overlay methods yield underestimated TOC values. Marcellus shale contains 48 Bcf of adsorbed gas and 74 Bcf of free gas in a drilling unit of one square mile. Free gas in the Marcellus shale ranges from 57% to 66% (approximately 2/3). This implies that Marcellus shale is composed of interconnected and organic matter porosity that are occupied by free gas.

Technically recoverable resources for the Marcellus shale were estimated using a recovery factor of 10%. Sonic/resistivity overlay, density/resistivity overlay, and density-based methods result in 11.29 Bcf, 14.38 Bcf, and 12.20 Bcf of technically recoverable resources for 640 acres area, respectively. The sonic/

resistivity overlay method provides a lower initial gas in place than the density/resistivity overlay method since sonic derived porosity is less than the density derived porosities. Difference in gas in place results can be attributed to the fact that we indirectly estimated the petrophysical properties using sonic, bulk density, and resistivity data. Moreover, our assumptions and input parameters can influence variations in porosity and hence gas in place results. As previously discussed, sonic logging cannot fully detect the extensive fracture network of the Marcellus shale. Additionally, relatively low compressional slowness measured by sonic logs, which is 91 μs/ft on average for organic matter and gas bearing Marcellus shale, can result in the difference between sonic and density derived porosities and gas in place results.

The Marcellus shale is heterogenous in terms of lithology, TOC, porosity, and geomechanical properties. Therefore, an efficient and effective fracturing treatment is required to increase recovery factor. Two stimulation candidate zones (Int_1 and Int_2) were identified which have relatively higher separations in porosity and resistivity log overlays, average TOC (3.2%), average porosity (8.8%), and potential technically recoverable resources (2.47 Bcf) in the upper and middle parts of the upper Marcellus member (Fig. 4). Moreover, the larger contrasts in minimum in situ stress and Young's modulus contrasts along the upper Marcellus-Stafford limestone boundary and lower part of the upper Marcellus member imply that the upper Marcellus member is an ideal candidate for stimulation treatments (Table 4). Additionally, a third stimulation candidate (Int_3) with relatively high separations in porosity and resistivity log overlays, TOC (2.0–7.1%), average porosity (9.0%), and potential technically recoverable resources (3.50 Bcf) was proposed in the lower part of the lower Marcellus member. The lower contact of the lower Marcellus member is not seen in the zone of interest (Fig. 4). However, a potential boundary between the lower Marcellus member and Onondaga limestone, as discussed by Lash and Engelder [5] with contrasts in minimum in situ stress and elastic modulus, can act as a barrier against fracture propagation.

In summary, Marcellus shale has a gas in place of 122 Bcf per square miles. The lower Marcellus member has two times resources in place than that of the upper Marcellus member. Free gas is approximately two times of the adsorbed gas. Resources estimate using the density-based method is the most accurate in the study area.

5 Conclusions

An in depth and comprehensive formation evaluation of shale gas formations was carried out to help optimize stimulation treatments and to increase economic recovery. Conclusions include:

- On the basis of our research and practical experiences in evaluating different geological formations, we developed a new formation evaluation method, including an improved workflow (Fig. 2) and a new unconventional petrophysical model (Fig. 3), to evaluate unconventional shale gas formations in five steps. We shared our experiences and lessons learned in evaluation of multi-scale multi-physics shale gas formations through a field case study.
- Out of the three methods available for TOC evaluation, density-based method is a preferred method in the evaluation of Marcellus shale compared to the resistivity/density and resistivity/sonic overlay methods. TOC of the upper Marcellus member (2.4%) is lower than that of the lower Marcellus member (3.0%). Additionally, the highest TOC (7.1%) was observed at the base of the lower Marcellus member. Average TOC is 2.8 wt% for the Marcellus in our study area.
- The modified density porosity model is more reliable than that from resistivity/density and resistivity/sonic overlay. Average porosity is 8.5% for the Marcellus in our study area. The lower Marcellus shale shows an average TOC of 3.0% and an average porosity of 8.8%, whereas the upper Marcellus shale has an average TOC of 2.4% and an average porosity of 7.8% based on our density-based method.
- Young's modulus and minimum in situ stress of the upper Marcellus member are 3.6 million psi and 2854 psi, respectively, while the Young's modulus and minimum in situ stress of the Stafford limestone are 4.6 million psi and 3747 psi, respectively. The large contrasts in minimum in situ stress and Young's modulus at the upper Marcellus-Stafford limestone boundary and lower part of the upper Marcellus member could serve as barriers for fracture height growth.
- The Marcellus shale has a gas in place of 122 Bcf per square miles. The lower Marcellus member has two times resources in place than that of the upper Marcellus member. Free gas is approximately two times of the adsorbed gas.
- In the Marcellus shale case study, three stimulation intervals were suggested by applying the methodology.

The new method and acquired knowledge help understand and evaluate shale gas reservoirs in the Marcellus shale in particular and in general globally, which can be applied to optimize stimulation treatments and increase economic recovery. Areas for further research include: (1) obtaining additional XRD data for the case study, (2) evaluating natural fractures through borehole image logs, and (3) incorporating core data to calibrate the TOC and porosity results.

Acknowledgment

The authors gratefully acknowledge the financial support of Turkish Petroleum Corporation, National Petroleum Exploration and Production Company of Turkey. The assistance of Paul Dudenas, manager of East Resources, in obtaining well log is appreciated.

Funding Data

- Turkish Petroleum Corporation.
- National Petroleum Exploration and Production Company of Turkey.

Conflict of Interest

There are no conflicts of interest.

Data Availability Statement

The datasets generated and supporting the findings of this article are obtainable from the corresponding author upon reasonable request.

Nomenclature

h = thickness, ft
p = reservoir pressure, psi
v = Poisson's ratio
A = cross-sectional area, ft^2
E = Young's modulus, psi
G = shear modulus, psi
K = bulk modulus, psi
R = true formation resistivity, ohm m
B_g = formation volume factor, ft^3/Scf
G_a = adsorbed gas in place, Bcf
G_c = adsorbed gas storage, Scf/ton
G_f = free gas in place, Bcf
G_r = technically recoverable resources, Bcf
G_t = initial gas in place, Bcf
P_l = Langmuir pressure, psi

R_B = resistivity on Δt_B when curves are baselined in clay rich rocks, ohm m
R_o = vitrinite reflectance, %
S_w = water saturation
V_{Cl} = volume of clay minerals
V_l = Langmuir volume, Scf/ton
$V_{P,Cl}$ = volume of pore space in clay minerals
V_{P,TOC_A} = volume of pore space in the organic matter whose pore space is occupied by adsorbed gas
V_{TOC} = volume of organic matter
V_{TOC_A} = volume of organic matter that is occupied by adsorbed gas
LOM = level of organic metamorphism
RF = recovery factor
TOC = total organic carbon, wt%
$TOC_{S,D}$ = total organic carbon from resistivity and sonic and density porosity log overlays, wt%
V_A, V_B, ..., V_J = volumes of fractions of solids and pore space in a shale gas reservoir
α = Biot poroelastic coefficient
$\Delta \log R$ = curve separation measured in logarithmic resistivity cycles
$\Delta \log R_D$ = curve separation between resistivity and density logs measured in logarithmic resistivity cycles
$\Delta \log R_S$ = curve separation between resistivity and sonic logs measured in logarithmic resistivity cycles
$\Delta \log R_{S,D}$ = curve separation between resistivity and porosity logs measured in logarithmic resistivity cycles
Δt = sonic log reading, μs/ft
Δt_B = compressional transit time in inorganic baseline interval, μs/ft
Δt_c = compressional slowness, μs/ft
Δt_{Cl} = sonic log reading in clay minerals, μs/ft
Δt_F = sonic log reading in fluids, μs/ft
Δt_{Ncl} = sonic log reading in non-clay minerals, μs/ft
Δt_s = shear slowness, μs/ft
Δt_{TOC} = sonic log reading in organic matter, μs/ft
ρ_b = bulk density, g/cm^3
ρ_{in} = density of inorganic intervals, g/cm^3
ρ_B = density value of baseline, g/cm^3
ρ_{Cl} = density of clay minerals, g/cm^3
ρ_{TOC} = density of organic matter, g/cm^3
ρ_{Ncl} = density of non-clay minerals, g/cm^3
ρ_F = fluid density, g/cm^3
σ_{min} = minimum in situ stress, psi
σ_{ob} = overburden stress, psi
σ_{tect} = tectonic stress, psi
ϕ_{Cl} = clay porosity
ϕ_{Den} = density porosity
ϕ_{Eff} = effective porosity
ϕ_{Son} = sonic porosity
ϕ_{TOC_A} = organic matter porosity that is occupied by adsorbed gas
ϕ_{Tot} = total porosity

References

[1] Osholake, T., Wang, J. Y., and Ertekin, T., 2013, "Factors Affecting Hydraulically Fractured Well Performance in the Marcellus Shale Gas Reservoirs," ASME J. Energy Resour. Technol., **135**(1), p. 013402.
[2] Zhou, D., Zheng, P., Peng, J., and He, P., 2015, "Induced Stress and Interaction of Fractures During Hydraulic Fracturing in Shale Formation," ASME J. Energy Resour. Technol., **137**(6), p. 062902.
[3] Chang, O., Kinzel, M., Dilmore, R., and Wang, J. Y., 2018, "Physics of Proppant Transport Through Hydraulic Fracture Network," ASME J. Energy Resour. Technol, **140**(3), p. 032912.
[4] Brett, C. E., and Baird, G. C., 1996, "Middle Devonian Sedimentary Cycles and Sequences in the Northern Appalachian Basin," Geol. Soc. Am. Spec. Pap., **306**, pp. 213–242.
[5] Lash, G. G., and Engelder, T., 2011, "Thickness Trends and Sequence Stratigraphy of the Middle Devonian Marcellus Formation, Appalachian Basin: Implications for Acadian Foreland Basin Evolution," AAPG Bull., **95**(1), pp. 61–103.
[6] Enomoto, C. B., Coleman, J. B., Haynes, J. T., and Whitmeyer, S. J., 2012, "Geology of the Devonian Marcellus Shale–Valley and Ridge Province, Virginia and West Virginia Field Trip Guidebook for the American Association of Petroleum Geologists Eastern Section Meeting, September 28–29, 2011," US Geological Survey, Report No. 2012-1194, 55, https://pubs.usgs.gov/of/2012/1194/pdf/ofr2012-1194.pdf
[7] Glorioso, J. C., and Rattia, A., 2012, "Unconventional Reservoirs: Basic Petrophysical Concepts for Shale Gas," SPE/EAGE Unconventional Resources Conference and Exhibition Held in Vienna, Austria, Mar. 20–22, Paper No. SPE-153004-MS.
[8] Asquith, G., and Krygowski, D., 2004, "Log Interpretation, in G. Asquith and D. Krygowski, Basic Well Log Analysis," AAPG Methods in Exploration, Tulsa, OK, p. 229.
[9] Wang, G., and Carr, T. R., 2013, "Organic-Rich Marcellus Shale Lithofacies Modeling and Distribution Pattern Analysis in the Appalachian Basin," AAPG Bull., **97**(12), pp. 2173–2205.
[10] Ambrose, R. J., Hartman, R. C., Campos, M. D., Akkutlu, I. Y., and Sondergeld, C. H., 2012, "Shale Gas-in-Place Calculations Part I: New Pore-Scale Considerations," SPE J., **17**(1), pp. 219–229.
[11] Alfred, D., and Vernik, L., 2012, "A New Petrophysical Model for Organic Shales," SPWLA 53rd Annual Logging Symposium, Cartagena, Colombia, June 16–20, Paper No. 2013-v54n3-A4.
[12] Ahn, C. H., Dilmore, R., and Wang, J. Y., 2017, "Modeling of Hydraulic Fracture Propagation in Shale Gas Reservoirs: A Three-Dimensional, Two-Phase Model," ASME J. Energy Resour. Technol., **139**(1), p. 012903.
[13] Zheng, H., Zhang, J., and Qi, Y., 2020, "Geology and Geomechanics of Hydraulic Fracturing in the Marcellus Shale Gas Play and Their Potential Applications to the Fuling Shale Gas Development," Energy Geosci., **1**(1–2), pp. 36–46.
[14] Meng, M., Ge, H., Shen, Y., and Ji, W., 2021, "Evaluation of the Pore Structure Variation During Hydraulic Fracturing in Marine Shale Reservoirs," ASME J. Energy Resour. Technol., **143**(8), p. 083002.
[15] Wang, J., Gu, D., Meng, X., and Yang, D., 2021, "Quantitative Characterization of Shale Porosities of Different Origins by Integrating Pore Genesis and Logging Analysis," ASME J. Energy Resour. Technol., **143**(10), p. 103004.
[16] Passey, Q. R., Bohacs, K. M., Esch, W. L., Klimentidis, R., and Sinha, S., 2010, "From Oil-Prone Source Rock to Gas Producing Shale Reservoirs-Geological and Petrophysical Characterization in Unconventional Shale-Gas Reservoirs," CPS/SPE International Oil & Gas Conference and Exhibition, Beijing, China, June 8–10, Paper No. SPE-131350-MS, 29.
[17] Sondergeld, C. H., Newsham, K. E., Comisky, J. T., Rice, M. C., and Rai, C. S., 2010, "Petrophysical Considerations in Evaluating and Producing Shale Gas Resources," SPE Unconventional Gas Conference, Pittsburgh, PA, Feb. 23–25, Paper No. SPE-131768-MS.
[18] Kim, T., Hwang, S., and Jang, S., 2016, "Petrophysical Approach for Estimating Porosity, Clay Volume, and Water Saturation in Gas-Bearing Shale: A Case Study From the Horn River Basin, Canada," Austrian J. Earth Sci., **109**(2), pp. 289–298.
[19] Milliken, K. L., Rudnicki, M., Awwiller, D. N., and Zhang, T., 2013, "Organic Matter–Hosted Pore System, Marcellus Formation (Devonian), Pennsylvania," AAPG Bull., **97**(2), pp. 177–200.
[20] Katahara, K. W., 1996, "Clay Mineral Elastic Properties," SEG Annual Meeting Expanded Technical Program Abstracts With Biographies, Denver, CO, Nov. 10–15, pp. 1691–1694.
[21] Ji, S., Wang, Q., and Xia, B., 2002, *Handbook of Seismic Properties of Minerals, Rocks and Ores*, Polytechnique International Press, Montreal, Quebec, p. 630.
[22] Rider, M. H., 1999, *The Geological Interpretation of Well Logs*, 2nd ed., Whittles Publishing Services, Caithness, p. 290.
[23] Haynes, W. M., 2014, *CRC Handbook of Chemistry and Physics*, 95th ed., CRC Press, Boca Raton, FL, p. 2666.
[24] Fertl, W. H., and Chilllger, G. V., 1988, "Total Organic Carbon Content Determined From Well Logs," SPE Form. Eval., **3**(2), pp. 407–419.
[25] Ward, A. J., 2010, "Kerogen Density in the Marcellus Shale," SPE Unconventional Gas Conference, Pittsburgh, PA, Feb. 23–25, Paper No. SPE-131767-MS.
[26] Vincké, O., Boutéca, M., and Longuemarre, P., 1998, "Investigation of the Poromechanical Behavior of Shales in Elastic Domain," SPE/ISRM Rock Mechanics in Petroleum Engineering, Trondheim, Norway, July 8–10, Paper No. SPE-47589-MS.
[27] Hart, D. J., and Wang, H. F., 1995, "Laboratory Measurements of a Complete Set of Poroelastic Moduli for Berea Sandstone and Indiana Limestone," J. Geophys. Res.: Solid Earth, **100**(B9), pp. 17741–17751.
[28] Starr, J., 2011, "Closure Stress Gradient Estimation of the Marcellus Shale From Seismic Data," SEG Technical Program Expanded Abstracts, Vol. 2011, pp. 1789–1793.
[29] Blood, D. R., McCallum, S. D., Jalali, J., Douds, A. S., and Stypula, M. J., 2020, "Towards a More Accurate Gas-in-Place Model: Reconciling Gas Storage With Gas Production in the Marcellus Shale, Appalachian Basin, USA," SPE/AAPG/SEG Unconventional Resources Technology Conference, Virtual, July 20, Paper No. URTEC-2020-2558-MS.
[30] Lemmon, E. W., Bell, I. H., Huber, M. L., and McLinden, M. O., 2010, "Thermophysical Properties of Fluid Systems," NIST Chemistry WebBook, NIST Standard Reference Database No. 69.
[31] Yu, W., and Sepehrnoori, K., 2013, "Simulation of Gas Desorption and Geomechanics Effects for Unconventional Gas Reservoirs," SPE Western Regional & AAPG Pacific Section Meeting 2013 Joint Technical Conference, Monterey, CA, Apr. 19, Paper No. SPE-165377-MS.

[32] Lecompte, B., Hursan, G., and Hughes, B., 2010, "Quantifying Source Rock Maturity From Logs. How to Get More Than TOC From Delta Log R," SPE Annual Technical Conference Exhibition, Florence, Italy, Sept. 20–22, Paper No. SPE-133128-MS.
[33] Passey, Q. R., Creaney, S., Kulla, J. B., Moretti, F. J., and Stroud, J. D., 1990, "A Practical Model for Organic Richness From Porosity and Resistivity Logs," AAPG Bull., **74**(12), pp. 1777–1794.
[34] Schmoker, J. W., 1993, "Use of Formation-Density Logs to Determine Organic-Carbon Content in Devonian Shales of the Western Appalachian Basin and an Additional Example Based on the Bakken Formation of the Williston Basin," *Petroleum Geology of the Devonian and Mississippian Black Shale of Eastern North America*, J. B. Roen, and R. C. Kepferle, eds., U.S. Geological Survey Bulletin, U.S. Government Printing Office, pp. J1–J14.
[35] Utley, L., 2005, "Unconventional Petrophysical Analysis in Unconventional Reservoirs—Putting the Puzzle Together in Gas Shales," SPWLA Houston Chapter Spring Seminar, Houston, TX, May.
[36] Wyllie, M. R. J., Gregory, A. R., and Gardner, L. W., 1958, "An Experimental Investigation of Factors Affecting Elastic Wave Velocities in Porous Media," Geophysics, **23**(3), pp. 459–493.
[37] Belyadi, H., Fathi, E., and Belyadi, F., 2019, *Hydraulic Fracturing in Unconventional Reservoirs: Theories, Operations, and Economic Analysis*, Gulf Professional Publishing, Cambridge, MA, p. 615.
[38] Dewan, J. T., 1983, *Essentials of Modern Open Hole Log Interpretation*, PennWell Corporation, Tulsa, OK, p. 361.
[39] Vatsa, T., and Wang, J. Y., 2011, "Fracture Height Containment in the Stimulation of Oriskany Sandstone," SPE Eastern Regional Meeting, Columbus, OH, Aug. 17–19, Paper No. SPE-149227-MS.
[40] Langmuir, I., 1918, "The Adsorption of Gases on Plane Surfaces of Glass, Mica and Platinum," J. Am. Chem. Soc., **40**(9), pp. 1403–1461.
[41] Seales, M. B., Ertekin, T., and Wang, J. Y., 2017, "Recovery Efficiency in Hydraulically Fractured Shale Gas Reservoirs," ASME J. Energy Resour. Technol., **139**(4), p. 042901.
[42] Bruner, K. R., and Smosna, R., 2011, "A Comparative Study of the Mississippian Barnett Shale, Fort Worth Basin, and Devonian Marcellus Shale, Appalachian Basin," Report to U.S. Department of Energy, Report No. DOE/NETL-2011/1478, https://permanent.fdlp.gov/gpo116992/DOE-NETL-2011-1478.pdf
[43] Godec, M., Koperna, G., Petrusak, R., and Oudinot, A., 2013, "Potential for Enhanced Gas Recovery and CO_2 Storage in the Marcellus Shale in Eastern United States," Int. J. Coal Geol., **118**, pp. 95–104.